RSC Advances

PAPER

View Article Online
View Journal | View Issue

Cite this: *RSC Adv.*, 2020, **10**, 37770

Cooperative physisorption and chemisorption of hydrogen on vanadium-decorated benzene†

Li-Juan Ma, ‡* Ting Han,‡ Jianfeng Jia and Hai-Shun Wu

Received 11th July 2020
Accepted 6th October 2020

DOI: 10.1039/d0ra06057g

rsc.li/rsc-advances

3d TM-decorated carbon composites have been proved to be a new generation of hydrogen storage materials. However, detailed hydrogen storage mechanisms are still unclear. Investigation of the H_2 dissociation and H migration on the 3d TM-decorated six-membered carbocycles is very critical for better understanding the hydrogen storage mechanism. In this paper, the processes of chemisorption and physisorption of multiple H_2 molecules on synthesized VC_6H_6 were simultaneously investigated for the first time. The Gibbs free energy calculations show that the optimal chemisorption pathway with the hydrogen storage capacity of 5.97 wt% is exothermic by 2.83 kcal mol^{-1}. Both the continuous hydrogenation giving the product of VC_6H_{11}–3H and reverse dehydrogenation could run smoothly at room temperature. The physisorption with a hydrogen storage capacity of 4.48 wt% will be exothermic by 13.49 kcal mol^{-1}. The H_2 molecules can be physisorbed at any temperature under 416 K and readily desorbed above 480 K at 1 atm. In summary, physisorption and chemisorption synergistically boost the hydrogen storage property of complex VC_6H_6. Our study provides a comprehensive picture of the interaction between hydrogen and VC_6H_6 and opens a new window for optimizing the future hydrogen storage materials.

1. Introduction

To satisfy the increasing global energy demands and solve serious environmental problems, renewable energy sources need to be researched to replace fossil-based fuels.[1] Hydrogen energy is reversible, recyclable, and pollution-free.[2,3] With the rapid progress of energy transformation, the value of hydrogen energy is further highlighted.[4–9] However, the hydrogen energy industry chain, especially the basic research on hydrogen storage links, faces many difficulties currently. Although many hydrogen storage methods[10–12] have their advantages in some aspects, they are not enough to meet the practical requirements of hydrogen energy in transportation. Generally, hydrogen is attached by physisorption or chemisorption. In physisorption, hydrogen remains in a molecular state and is weakly bound to the surface. In chemisorption, H_2 molecules dissociate into double H atoms and even migrate to the material forming chemical bonds, which are strong.[6] Kubas-type orbital interaction[13,14] is similar to physisorption, in which the H–H bond in an H_2 molecule is elongated but not broken. It improves the hydrogen adsorption energy of transition metals (TMs)-decorated carbon composites (0.10–0.80 eV)[6] and makes most of the hydrogen gravimetric storage capacities satisfy the target of the U.S. Department of Energy (~6.5 wt%).[15] Then, TM-decorated carbon composites grew up to be a new generation of hydrogen storage materials.[16–19] Interestingly, the dissociation of the first H_2 was spontaneous on most of Sc/Ti/V-decorated carbon nanostructures.[20–22] The dissociation of the H_2 increases the probability of H migration. The question then arises: whether hydrogen molecules are adsorbed only or migrate to form C–H bonds? If dissociation and even migration take place and TM-H/C–H bond is formed, the adsorption of H_2 on transition-metal-decorated nanomaterials will change from physisorption to chemisorption. Investigation of the H_2 dissociation and H migration is very important for better understanding the hydrogen storage mechanism on the 3d transition metal-decorated carbon nanostructures. While physisorption was mainly focused on and chemisorptions was always neglected.

On the other hand, the spillover mechanism is another promising mechanism for enhancing the H_2 uptake in carbon-based materials.[23–25] Hydrogen spillover following three processes: (1) the dissociation of H_2 molecules on the TM sites; (2) the migration of the atomic hydrogen from TM sites to the carbon surface and (3) the diffusion of atomic hydrogen on the carbon surface eventually forming a stable C–H bond. Understanding these three key steps is necessary to fully understand the hydrogen spillover process. Most theoretical studies on the

Key Laboratory of Magnetic Molecules & Magnetic Information Materials Ministry of Education, School of Chemical and Material Science, Shanxi Normal University, No. 1, Gongyuan Street, Linfen, China, 041004. E-mail: malijuan19852223@163.com; malijuan@sxnu.edu.cn

† Electronic supplementary information (ESI) available. See DOI: 10.1039/d0ra06057g

‡ These authors contributed equally to this work and should be considered co-first authors.

mechanism of hydrogen spillover on carbon adsorbent have been carried out on graphene.[26–30] The metal catalyst is an important factor affecting storage by hydrogen spillover. So far, the dissociation sources for hydrogen spillover have been long known for TMs such as Pt, Pd, Ru, Ni, and Ti.[31–34] The experimental progress of Kubas-type H_2-storage materials always confirmed by V-containing polymers.[35] Then, could monatomic V be used as a source of dissociation sources for hydrogen spillover?

Six-membered carbocycle isan important linker in some metal organic frameworks[36,37] and covalent organic frameworks[38] but also a basic unit of C_{60},[39,40] graphene,[41,42] and carbon nanotubes.[43–46] In this regard, Ti/Sc/V-benzene complexes as representative units of high-capacity hydrogen storage materials have received great attention.[47–50] In this study, based on first-principles calculations, the adsorption behavior of hydrogen on the synthesized VC_6H_6 (ref. 51–54) is focused on to further address the hydrogen storage mechanism. Previously, Weck,[47] Ajay,[48] and Li[49] reported that VC_6H_6 could adsorb three hydrogen molecules, but the only physisorption was considered. Here, a systematic study of both physisorption and chemisorption is investigated. The mechanism of dissociative adsorption and even the migration of the H atoms on VC_6H_6 is investigated. It was found that physisorption and chemisorption synergistically boost the hydrogen storage property of complex VC_6H_6. Most of our findings would have a great significance for the study of hydrogen storage on TM-decorated carbon composites.

2. Computational methods and details

All geometry optimizations were carried out by using the density functional theory (DFT) method at B3LYP[55]/6-31+G(d,p) level. The whole calculations employed the Gaussian 09 suite of programs.[56] The optimization was carried out without any symmetry constraint and different spin multiplicities were considered. The optimized geometric coordinates and energies were listed in the ESI.† Frequency calculations were performed to confirm that there was no imaginary frequency in the stable structure, and one imaginary frequency in the transition states. *Ab initio* molecular dynamics (MD) simulations based on atom density matrix propagation (ADMP)[57–61] were performed to confirm part of the favorable dissociation paths.

Consecutive adsorption energies with ZPEs (ΔE_n) and Gibbs free energy corrections (ΔG_n) at 298.15 K were obtained using the following formula:

$$\Delta E_n = E(VC_6H_6(H_2)_{n-1}) + E(H_2) - E(VC_6H_6(H_2)_n) \quad (1)$$

$$\Delta G_n = G(VC_6H_6(H_2)_{n-1}) + G(H_2) - G(VC_6H_6(H_2)_n) \quad (2)$$

where E(X) is the sum of electronic and zero-point energy, G(X) is the sum of electronic and thermal free energy of the corresponding structure at 298.15 K, n represents the number of H_2 molecules.

In the equilibrium state, various conformations of $VC_6H_6(H_2)_n$ have different energy and proportion. The proportion of conformation (P_i) was calculated according to the Boltzmann distribution:

$$P_i = N_i\left(\sum_j N_j\right)^{-1} = e(-E_i/RT)\left(\sum_j e(-E_j/RT)\right)^{-1} = Q_iQ^{-1} \quad (3)$$

where N is the number of conformation, E is the energy of conformation, T represents the temperature (Kelvin), R is the ideal gas constant, and Q is the partition function.

Spin multiplicity, vibrational frequencies, ionization energy, and electron affinity of VC_6H_6 were calculated to test the reliability of our calculations. The range-separated hybrid DFT method (wB97XD)[57] was used. The larger Pople-style orbital basis sets 6-311G++(3df,3pd) and diffuse functions in standard basis set aug-cc-pVTZ for C, H, and large-core relativistic Stuttgart–Dresden effective core potential(SDD)[58] basis set for V atom were included.

As shown in Table 1, both the results using B3LYP/6-31G+(d,p) and wB97XD/6-311G++(3df,3pd) show that VC_6H_6 is quartet state and the vibrational frequencies of VC_6H_6 are in good agreement with the experimental values.[48] The ionization energies and electron affinities of VC_6H_6 in Table 2 using B3LYP/6-31G+(d,p), B3LYP/aug-cc-pVTZ and wB97XD/6-311G++(3df,3pd) are in good agreement with the experimental values in ref. 51 and 53. The C–C bond lengths and the C–H bond lengths of VC_6H_6 using B3LYP/6-31+g(d,p) are 1.40–1.56 Å and 1.08–1.10 Å, respectively, which coincide well with the theoretical results by Duncan.[54] These values indicate the scheme of B3LYP/6-31+g(d,p) is a good compromise between accuracy and computational effort.

Moreover, the adsorption processes of H_2 molecules on TM decorated carbon nanomaterials include Kubas-type bonding, H_2 dissociation, H atom migration, and even strong C–H bonds producing. Both our previous researches[52] and other group's reports[59–61] prove that the B3LYP method is appropriate for obtaining both reliable structures and potential energy surfaces. Firstly, B3LYP functional is very valid for estimating the H_2 storage property of Ti-acetylene/ethylene compounds.[59–61] Secondly, the B3LYP method employing a 6-31+G(d,p) basis set was used to study the hydrogen storage capacity of alkali metal ion decorated boric acid.[62] Thirdly, the investigation of the stepwise adsorption energies of hydrogen on TiC_6H_6 showed the M06-2X functional was not preferred and the B3LYP functionals with 6-31+g(d,p) basis sets gave an impressive agreement with the accurate results.

3. Results and discussion

3.1 Optimized configurations of $VC_6H_6(H_2)_n$ (n = 1–4)

Optimized configurations of $VC_6H_6(H_2)_n$ (n = 1–4) and relative free energies at 298.15 K and 1 atm are presented in Fig. 1, 3–5, respectively. Thermodynamic data show that the configurations in the quartet state are lower in energy than the corresponding doublet state except for **1c**. The most stable structure is the **1a**(Q), which is 8.25 kcal mol^{-1} lower in energy than the doublet state. **1a** with the dissociated H_2 molecule is mentioned in ref.

Table 1 Spin multiplicity, energy differences Δ (in eV) between doublet state and quartet state, and vibrational frequencies of VC_6H_6 (in cm^{-1})

Functional	Multi.	Δ (eV)	$\nu_{o\text{-}p}$(CH)[a]	ν_s(CC)	$\nu_{i\text{-}p}$(CH)	ν(CC)
B3LYP/6-31G+(d,p)	2	0.07				
	4	**0.00**	**769.05**	**956.3**	**1319.34**	**1420.15**
B3LYP/6-311G++(3df,3pd)	2	0.30				
	4	**0.00**	**734.10**	**924.20**	**1368.27**	**1507.34**
B3LYP/aug-cc-pVTZ	2	0.11				
	4	**0.00**	**679.54**	**928.29**	**1341.32**	**1500.48**
wB97XD/6-311G++(3df,3pd)	2	2.64				
	4	**0.00**	**760.51**	**947.81**	**1329.71**	**1426.20**
wB97XD/aug-cc-pVTZ	2	1.61				
	4	**0.00**	**781.87**	**974.09**	**1348.03**	**1506.89**
Experiments[54]			758.00	958.00	1306.00	1460.00

[a] Vibrational modes: $\nu_{o\text{-}p}$(CH) = C–H out of plane bending; ν_s(CC) = symmetric C–C stretching; $\nu_{i\text{-}p}$(CH) = C–H in-plane rocking; ν(CC) = asymmetric C–C stretching.

Table 2 Ionization energy (eV) and electron affinity (eV) of VC_6H_6

Functional	Ionization energy (eV)	Electron affinity (eV)
B3LYP/6-31+G(d,p)	**6.44**	0.62
B3LYP/6-311G++(3df,3pd)	**6.46**	0.40
B3LYP/aug-cc-Pvtz	**6.44**	**0.65**
wB97XD/6-311G++(3df,3pd)	**6.59**	**0.65**
wB97XD/aug-cc-pVTZ	**5.98**	0.70
Experiments	6.30 ± 0.50 (ref. 51)	0.62 ± 0.07 (ref. 53)

31 **1b** with the CH_2 group is more stable than the **1c** with molecular H_2. It indicates hydrogen dissociation, H migration, and even formation of the C–H bond are favorable thermodynamically. Chemisorption forming C–H or V–H bonds is usually stronger than physisorption forming V–H_2 unit. Then, it's easy to understand that structure **1a** with V–H bonds and **1b** with a C–H bond is more stable than structure **1c**. The configurations of **1d**, **1e**, and **1f** have two CH_2 groups. The original C_6H_6 has a little deformation and the longest V–C bond length increases from 2.32 Å to 2.94 Å due to the formation of the CH_2 groups. Obviously, the forming of the C–H bond causes a great deformation of the C_6H_6 unit. The preferred site of one H atom in VC_6H_6 is determined by comparing the two structures in Fig. S2.† The binding energy of H to the V site is 2.83 eV, which is larger than that of H to the C site (1.82 eV). This indicates that the H atoms prefer to bind at the on-top V site. That's maybe why **1a** with the V–H bonds is more stable than **1b** with a C–H bond.

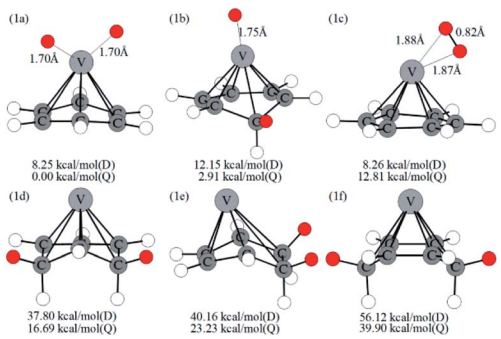

Fig. 1 Optimized configurations of VC_6H_6–H_2 at the B3LYP/6-31+G(d,p) level and relative free energies at 298.15 K (in kcal mol^{-1}). D and Q represent the doublet state and quartet state, respectively. The red circle means adsorbed hydrogen.

The dissociation of the first H_2 was spontaneous on most of Sc/Ti/V decorated carbon nanostructures.[35–42] To understand the dissociation process, Fig. 2 shows the partial orbital density state (PDOS) of V and adsorbed H_2 in **1c** ($VC_6H_6(H_2)$), and **1a** ($VC_6H_6(2H)$). Effective intermolecular bonding leads to bonding orbits have lower energies. Two parts interact strongly when electrons filling in these bonding orbits. The three principles of effective bonding include matching symmetry, energy proximity, and maximum overlap between orbits. For **1c**, the orbital in the energy of −13.00 eV mainly comes from the s orbits of H_2 and the other orbitals of VC_6H_6 are almost unaffected by the hydrogen molecule. The larger energy difference between the orbitals from V and the H_2 causes weak interaction. For **1a**, the localized 3d orbits of V in VC_6H_6 mix with s orbits from hydrogen atoms easily in energies of −6.00–7.50 eV. So, VC_6H_6 has a strong interaction with the H atoms rather than a hydrogen molecule.

The structures in Fig. 3 include the configurations with one CH_2 group (**2d**), two CH_2 groups (**2e**, **2g**, **2h**), and three CH_2 groups (**2a**, **2f**, **2i**). The **2b** structure contains an activated hydrogen molecule and two V–H bonds, which was mentioned in previous literature.[40] **2a** and **2b** structures have an energy difference of only 0.14 kcal mol^{-1} at the B3LYP level.

This little energy difference indicates **2b** inclines to form more stable **2a**. For the structure shown in Fig. 3, the bond length of the V–H bond is 1.67–1.74 Å for isomers with one H atom but is 1.90–1.95 Å for isomers with H_2, which is longer than the former. This means that the single H atom has a stronger interaction with metal V. The distance of C–C neighboring CH_2 is lengthened to 1.50–1.56 Å. Besides, the V–C

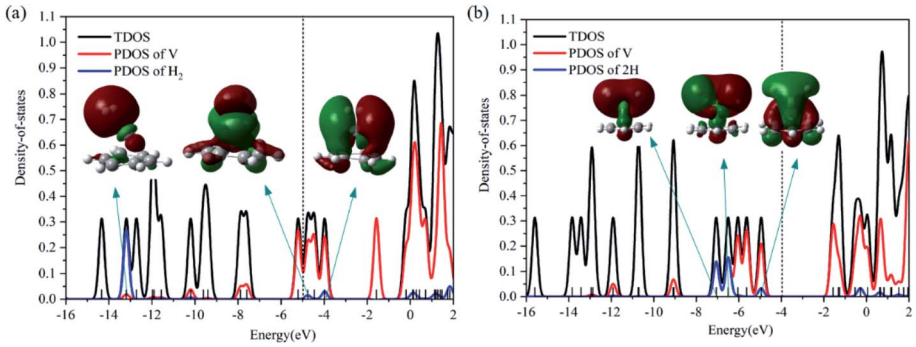

Fig. 2 The total DOS of (a) **1c**($VC_6H_6(H_2)$), (b) **1a**($VC_6H_6(2H)$) and the PDOS of V and H_2.

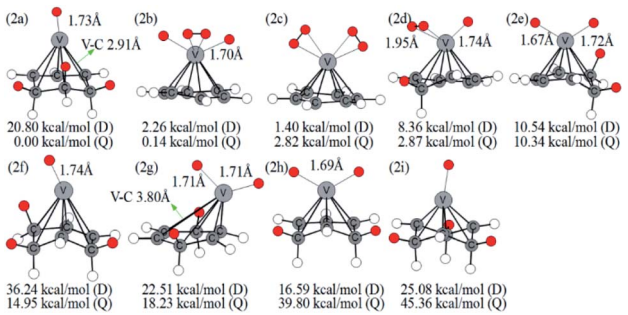

Fig. 3 Optimized configurations of various isomers of VC_6H_6–$2H_2$ at the B3LYP/6-31+G(d,p) level and relative Gibbs free energies at 298.15 K (in kcal mol^{-1}). The red circle means adsorbed hydrogen.

bond adjacent to three CH_2 groups in **2a** is stretched from 2.28 Å to 2.91 Å, and causing the metal V atom is tilted to one side.

The optimized $VC_6H_6(H_2)_3$ are displayed in Fig. 4. Notably, the **3a** with not CH_2 groups is the most stable doublet isomer due to its higher symmetry (C_{3V}). From the perspective of overlooking, it can be seen that the position of H_2 molecules corresponds to the C–C bond in the six-membered ring. There are two configurations with one CH_2 group (**3e**, **3f**), six configurations with two CH_2 groups (**3i**, **3l**, **3m**, **3n**, **3p**, **3q**), five configurations with three CH_2 groups (**3d**, **3g**, **3j**, **3o**, **3r**), and three configurations with four CH_2 groups (**3b**, **3h**, **3k**). Thus, the structures with the adjacent CH_2 groups are more stable.

A complex containing dissociated H_2 molecules (with V–H bond) is always more stable than the corresponding complex with activated H_2 molecules. For example, **1a** with the dissociated H_2 molecule is more stable than the **1c** with molecular H_2; the **2b** structure contains an activated hydrogen molecule and two V–H bonds is more stable than the **2c** with two molecular H_2 and so on. However, the reverse appears in the $VC_6H_6(H_2)_3$ isomers. Firstly, calculations at different theoretical levels confirm our results. As shown in Table S2,† both the results

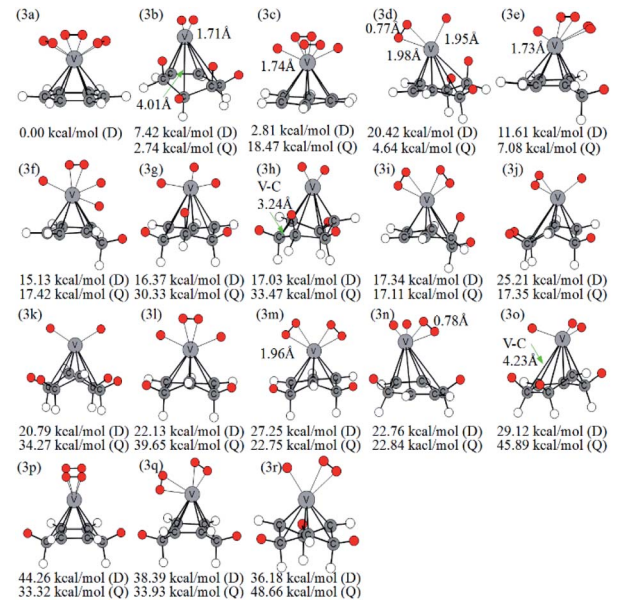

Fig. 4 Various configurations of VC_6H_6–$3H_2$ at the B3LYP/6-31+G(d,p) level and relative Gibbs free energies at 298.15 K (in kcal mol^{-1}). The red circle means adsorbed hydrogen.

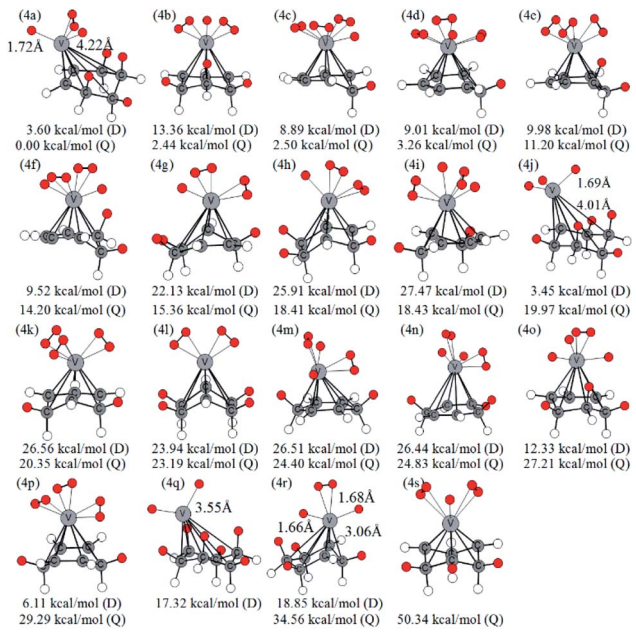

Fig. 5 Optimized configurations of various isomers of VC_6H_6–$4H_2$ at the B3LYP/6-31+G(d,p) level and relative Gibbs free energies at 298.15 K (in kcal mol^{-1}). The red circle means adsorbed hydrogen.

using B3LYP/6-31G+(d,p), B3LYP/6-311G++(3df,3pd), B3LYP/aug-cc-pVTZ, wB97XD/6-311G++(3df,3pd) and wB97XD/6-311G++(3df,3pd) show that **3a** with three molecular H_2 molecules is more stable than the **3c** with the dissociated H_2 molecule. Secondly, detailed analyses of the symmetry and energy of deformation are carried out to comment on why this is the case. The symmetry of optimized VC_6H_6(D) is C_{6V}. As shown in Table S2,† the VC_6H_6 unit in structure **3a** is C_{6V} symmetry while that in structure **3c** is C_2 symmetry. That's mean, after adsorbing $3H_2$, the VC_6H_6 unit in structure **3a** is nearly no change. Therefore, the energy of deformation (ΔG_R) of VC_6H_6 and hydrogen binding energy between the VC_6H_6 unit and $3H_2$ unit in **3a** and **3c** (ΔG_H) are defined.

$$\Delta G_R = G(VC_6H_6 \text{ unit in } \mathbf{3a/3c}) - G(VC_6H_6)$$

$$\Delta G_H = [G(VC_6H_6 \text{ unit in } \mathbf{3a/3c}) + G(3H_2 \text{ unit in } \mathbf{3a/3c}) - G(\mathbf{3a/3c})]/3$$

The values of ΔG_R and ΔG_H are listed in Table S3.† The deformation energy of **3c** is 0.28 eV, which is greater than that of **3a** (0.23 eV). When deformation energy is not taken into account, the hydrogen binding energy between the VC_6H_6 unit in **3c** and $2H_2$–2H unit is 2.52 eV, which is greater than that between the VC_6H_6 unit in **3a** and $3H_2$(0.72 eV). This is consistent with the common understanding.

Similarly, Fig. 5 lists several optimized isomers of VC_6H_6–$4H_2$ complexes. Notably, the structure with four activated hydrogen molecules is very unstable. The most stable configuration **4a** is composed of four adjacent CH_2 groups with an activated hydrogen molecule and two H atoms. Among many other configurations, **4c**, **4d**, and **4f** have one CH_2 group are, **4e**, **4i**, **4k**, **4m**, and **4p** have two CH_2 groups, **4b**, **4g**, **4h**, **4n**, **4o**, and **4s** have three CH_2 groups, **4a**, **4l**, and **4r** have four CH_2 groups, **4j** has five CH_2 groups, and **4q** has six CH_2 groups. The energy difference between **4g** and **4h** is 3.05 kcal mol^{-1}, though both have three CH_2 groups and two activated hydrogen molecules. It indicates that the energy of structures also depends on the direction of the activated hydrogen molecule. **4q** and **4j** have six and five consecutive CH_2 groups, respectively, but their energy is not the lowest. This may be due to the steric hindrance effect formed by the consecutive CH_2 groups. For VC_6H_6–nH_2 (n = 1, 3), the most stable isomers have no CH_2 group. For VC_6H_6–nH_2 (n = 2,4), the most stable isomers have CH_2 groups, and in which CH_2 groups are adjacent. These prompt us to think strongly about whether the C–H bond could be formed easily.

3.2 The optimal chemisorption pathway of multiple H_2 molecules on the VC_6H_6

3.2.1 Chemisorption of the first H_2 molecule. As shown in Fig. 6, VC_6H_6 adsorb the first H_2 in molecular form firstly. The single H_2 dissociates into two H atoms *via* the TS **1c/1a**. For the quartet state, the dissociation is exothermic by 13.22 kcal mol^{-1}, and its barrier is only 2.72 kcal mol^{-1}. For the doublet state, the dissociation is endothermic by 0.02 kcal mol^{-1}, and its barrier is 6.53 kcal mol^{-1}. It indicates

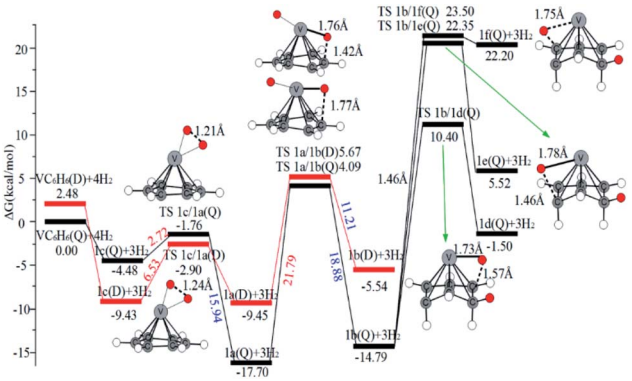

Fig. 6 The Gibbs free energy profiles of the first H_2 molecule adsorbed on VC_6H_6. The red and black lines represent doublet (D) and quartet (Q) states, respectively. The energy barriers are highlighted in red for the forward reaction and blue for the backward reaction.

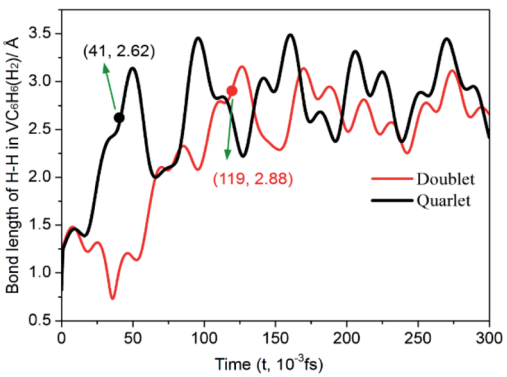

Fig. 7 Time evolution trajectories of the H–H in $VC_6H_6(H_2)$ at 300 K. The bond lengths are given in Å.

that the H_2 dissociation in **1c**(Q) is more favorable than that in **1c**(D), which is also confirmed by the first-principles molecular-dynamics MD simulations up to 0.3 fs. The time evolution trajectories of H–H in $VC_6H_6(H_2)$ at 300 K are presented in Fig. 7. After 0.04 fs, the H–H bond in **1c**(Q) elongates from 0.824 Å to 2.621 Å (the length of the H–H bond in **1a**(Q)). While H–H bond in **1c**(D)is shortened firstly and then elongates from 0.869 Å to 2.876 Å (the length of H–H bond in **1a**(D)) until 0.12 fs.

One of the dissociated H atoms in **1a**(Q) will migrate to form CH_2 group with a barrier of 21.79 kcal mol^{-1}, which is endothermic by 2.91 kcal mol^{-1} and slow. At 298.15 K, the overall conformation analysis shows that the **1a**(Q) and **1b**(Q) of VC_6H_6–H_2 are 99.3% and 0.70%, respectively. IR stability calculations ensure that the structures **1a**(Q) and **1b**(Q) are energy minima without imaginary frequency (see Fig. S4 of the ESI†). Two main H modes for **1a**(Q) are symmetric and anti-symmetric stretching vibrations, respectively corresponding frequencies of 1606.48 and 1645.80 cm^{-1}. One main H mode vibration frequency for **1b**(S) is 1582.26 cm^{-1}. The three unique modes should be present in the Raman/IR spectra of a successfully synthesized material.

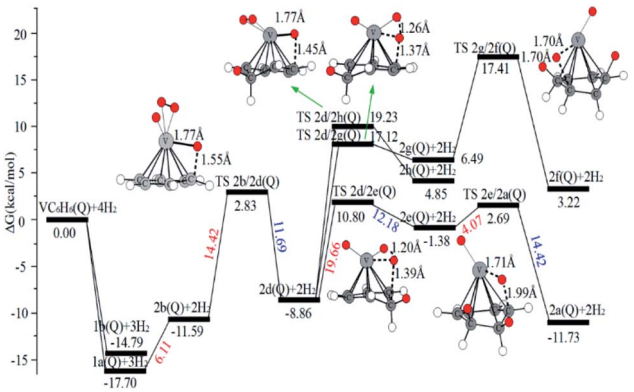

Fig. 8 The Gibbs free energy profiles of the second H_2 molecule adsorption on the VC_6H_6 complex. The energy barriers are highlighted in red for the forward reaction and blue for the backward reaction.

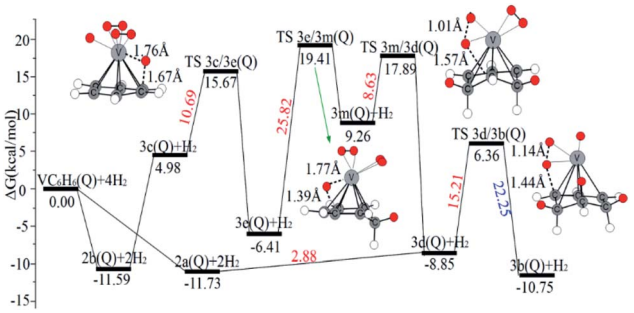

Fig. 9 The Gibbs free energy profiles of the third H_2 molecule adsorption on the VC_6H_6 complex. The energy barriers are highlighted in red for the forward reaction and blue for the backward reaction.

3.2.2 Chemisorption of the second H_2 molecule. The intermediate **1a**(Q) is the precursor of the second H_2 molecule adsorption (Fig. 8). **2b**(Q) dihydrogen complex is formed by the H_2 molecule adsorption on V atom in **1a**(Q). H atom in **2b**(Q) migrates to C atom through TS **2b**/**2d**(Q) with a barrier of 14.42 kcal mol^{-1}. Another H atom on **2d**(Q) continues to migrate to form the other CH_2 group in **2e**(Q). The reaction barrier of **2e**(Q) → **2a**(Q) is 4.07 kcal mol^{-1}. The energy difference between **2a**(Q) and **2b**(Q) is 0.14 kcal mol^{-1}, which is very small. Similarly, conformations population analysis at 298.15 K shows that **2a**(Q) and **2b**(Q) account for 55.83% and 44.17%, respectively, which indicates they can coexist. The formations of **2g**, **2h**, and **2f** are unfavorable due to they are endothermic.

3.2.3 Chemisorption of the third and the fourth H_2 molecules. There are a series of processes including hydrogen molecules adsorption, hydrogen molecules dissociate, and H atomic migration. It was observed in Fig. 9 that the process from **2b**(Q) to **3b**(Q) has energy barriers of 25.82 kcal mol^{-1}. There is another easier pathway from **2a**(Q), in which the H_2 molecule can be absorbed on the V atom to form **3d**(Q). Compared with **2b**(Q) + H_2 → **3c**(Q), **2a**(Q) + H_2 → **3d**(Q) is more favorable. The H_2 molecule in **3d**(Q) can be dissociated. At the same time, one H atom of the H_2 molecule migrates with the barrier of 15.21 kcal mol^{-1}.

When the fourth H_2 molecule continues to approach the structure **3b**(Q), the consecutive adsorption energies (ΔE_n-ZPE) is 2.18 kcal mol^{-1} (0.09 eV). The **4a**(Q) forms **4j**(D) through a spin crossover. When **4j**(D) is used as a reactant, it is unfavorable to generate **4q**(D) (Fig. 10).

The optimal chemisorption pathways of H_2 molecules on VC_6H_6 are shown in Fig. 11. (More detailed information regarding optimized cartesian coordinates and computed sum of electronic and thermal free energies of mentioned structures see the ESI†). When the pressure of hydrogen increases, H_2 molecules adhering to VC_6H_6 can migrate continuously to form CH_2 groups, and finally VC_6H_{11}–3H (**4j**) is formed. Gibbs free energy calculations show that the whole reaction is exothermic by 2.83 kcal mol^{-1} at 298.15 K. The generation of **4q**(D) is endothermic by 11.14 kcal mol^{-1}, which is unfavorable in thermodynamics. The dissociation and migration of the second H_2 is the rate-determining step in the whole reaction with a barrier of 19.66 kcal mol^{-1}. In turn, the complex VC_6H_{11}–3H will dehydrogenate continuously until VC_6H_6 when the hydrogen pressure decreases. The energy barrier of the critical speed step (the migration of H atom in **3d**(Q)) is 17.11 kcal mol^{-1}. Hence the hydrogen chemisorption adsorption and desorption on the VC_6H_6 complex could run smoothly with the hydrogen storage of 5.97 wt%, simply regulated by increasing/decreasing the hydrogen pressure.

As the discussion above, the chemisorptions pathway of H_2 molecules on VC_6H_6 at 298.15 K indicates that: (1) H_2 molecules attached to VC_6H_6 can be dissociated, and H atoms migrate continuously to form CH_2 groups. (2) Spin crossover mainly occurs in the pathway of adsorption of the first and fourth hydrogen molecules. (3) The optimal chemisorption pathway should be VC_6H_6(Q) → **1c**(D) → **1a**(Q) → **2b**(Q) → **2d**(Q) → **2e**(Q) → **2a**(Q) → **3d**(Q) → **3b**(Q) → **4a**(Q) → **4j**(D) (VC_6H_{11}–3H). (4) Gibbs free energy calculations show that the overall reaction to give the hydrogenation product **4j** (VC_6H_{11}–3H) is exothermic by 2.83 kcal mol^{-1} and has an energy barrier of 19.66 kcal mol^{-1}.

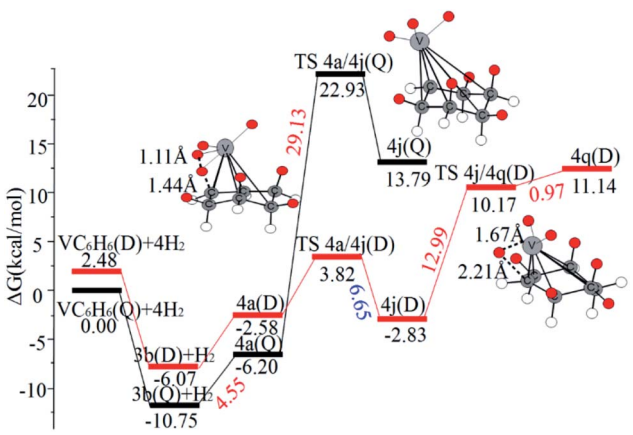

Fig. 10 The Gibbs free energy profiles of the fourth H_2 molecule adsorption on VC_6H_6. The energy barriers are highlighted in red for the forward reaction and blue for the backward reaction.

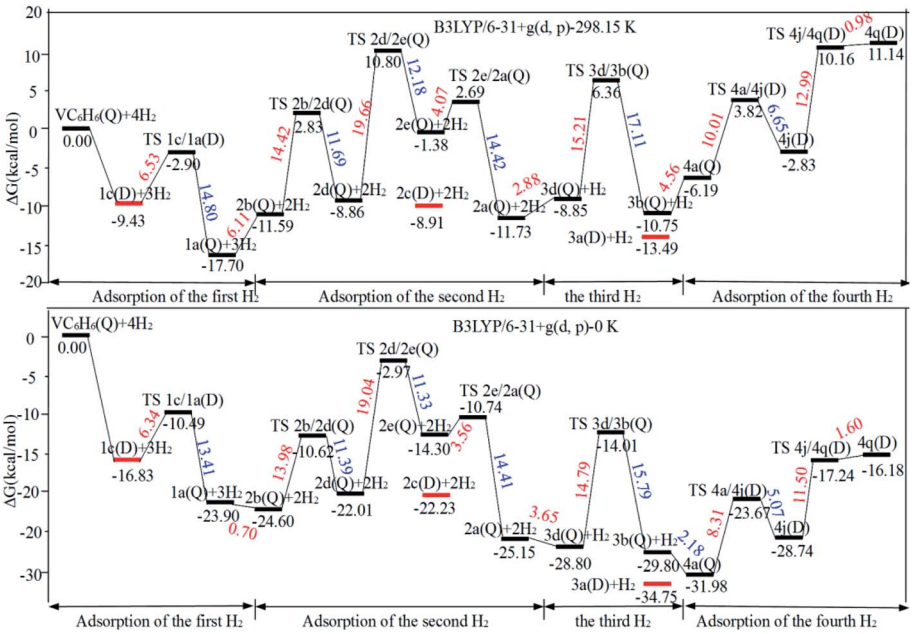

Fig. 11 The optimal chemisorption and physisorption pathways of H_2 molecules on VC_6H_6 at 298.15 K and 0 K. The energy barriers are highlighted in red for the forward reaction and blue for the backward reaction. The red line corresponds to the physisorption structures.

3.3 Physisorption of multiple H_2 molecules on the VC_6H_6

Fig. 12a shows the optimal physical adsorption path of multiple H_2 molecules on the VC_6H_6 complex. The free energy profile is shown in Fig. S5.† For $n = 1$, H_2 dissociates into two H atoms *via* the transition state TS. Though the single H_2 dissociation on VC_6H_6 is exothermic, the dissociation barrier is 6.34 kcal mol^{-1}. Moreover, **3a** is more stable than **3c**. So, the adsorption pathway along VC_6H_6 → **1c**(D) → **2c**(Q) → **3a**(Q) pathway will be more favorable thermodynamically.

When all the three hydrogen molecules are adsorbed in molecular form, the consecutive adsorption energies are 0.50, 0.56, 0.45 eV, respectively. And the average hydrogen adsorption energy for $VC_6H_6(H_2)_3$ is 0.50 eV, which is between physisorption and chemisorption (0.20–0.60 eV). As shown in Fig. 11, the physisorption of the three hydrogen molecules is exothermic by 13.49 kcal mol^{-1} at 298.15 K, and need no energy barrier. The hydrogen storage capacity of VC_6H_6 is 4.48 wt%. Based on the van't Hoff equation: $TD = (E_a/k_B)(\Delta S/R - \ln P)^{-1}$,[63] the three H_2 can be adsorbed at any temperature under 421 K and 1 atm. Notably, spin multiplicity and the Gibbs free energy correction fully considered here. The temperatures at which $\Delta G = 0$ eV/H_2 for **1c**(Q), **2c**(Q), **3a**(D) are 480 K, 462 K, and 416 K, respectively (Fig. 12b). It also indicates that three H_2 molecules can be spontaneously adsorbed on VC_6H_6 forming **3a** below 416 K. And three H_2 can be readily desorbed above 480 K under atmospheric pressure.

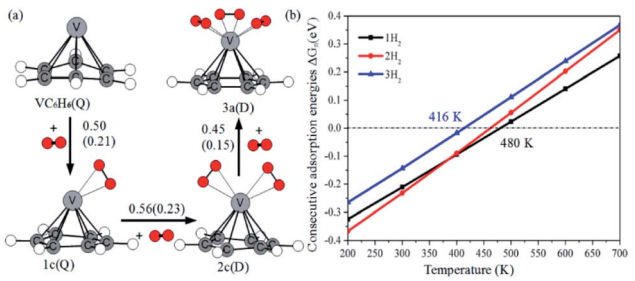

Fig. 12 (a) The consecutive adsorption energies ΔE_n (ΔG_n) of multiple H_2 molecules on the VC_6H_6 (in eV), (b) temperature dependence of ΔG_n at $p = 1$ atm.

4. Conclusions

TM-decorated carbon composites grew up to be a new generation of hydrogen storage materials. Most of these researches reported that the dissociation of the first H_2 was spontaneous on most of Sc/Ti/V-decorated carbon nanostructures. As known that H migration easily occurs on metal sites. Then hydrogenation reaction would also occur during the hydrogen storage on 3d TM-decorated organic complexes. To further address this issue, the process of hydrogen adsorption on synthesized VC_6H_6 is focused on answering the question that whether hydrogen molecules are absorbed only or migrate to form C–H bonds.

Optimized configurations of $VC_6H_6(H_2)_n$ (n = 1–4) and relative Gibbs free energies at 298.15 K and 1 atm were presented. For VC_6H_6–nH_2 (n = 1, 3), the most stable isomers have no CH_2 group. For VC_6H_6–nH_2 (n = 2,4), the most stable isomers have adjacent CH_2 groups. The chemisorptions pathway of H_2 molecules on VC_6H_6 at 298.15 K indicates that H_2 molecules attached to VC_6H_6 can be dissociated, and H atoms migrate continuously to form CH_2 groups. Gibbs free energy calculations show that the overall reaction giving the hydrogenation product **4j** (D) (VC_6H_{11}–3H) is exothermic by 2.83 kcal mol^{-1} and has an energy barrier of 19.66 kcal mol^{-1}. Hence the

hydrogen chemisorption adsorption and desorption on the VC_6H_6 complex could run smoothly with the hydrogen storage of 5.97 wt%, simply regulated by increasing/decreasing the hydrogen pressure. The physisorption along VC_6H_6 → **1c**(D) → **2c**(Q) → **3a**(Q) will be exothermic by 13.49 kcal mol^{-1}. The three H_2 can be adsorbed at any temperature under 416 K and readily desorbed above 480 K at 1 atm. The corresponding hydrogen storage capacity is 4.48 wt%. In summary, both physisorption and chemisorption tend to occur in certain circumstances.

Conflicts of interest

There are no conflicts to declare.

Acknowledgements

This work is financially supported by the National Natural Science Foundation of China (21805176), the 1331 Engineering, and Education Reform Project (J2019098) and Youth Science and Technology Research Foundation (201901D211394) of Shanxi Province of China, the Doctor Fund (0505/02070359) of Shanxi Normal University.

Notes and references

1 I. L. R. Gomes, H. M. I. Pousinho, R. Melicio and V. M. F. Mendes, *Energy*, 2017, **124**, 310–320.
2 S. Niaz, T. Manzoor and A. H. Pandith, *Renewable Sustainable Energy Rev.*, 2015, **50**, 457–469.
3 A. G. Stern, *Int. J. Hydrogen Energy*, 2018, **43**, 4244–4255.
4 K. T. Møller, T. R. Jensen, E. Akiba and H.-w. Li, *Prog. Nat. Sci.: Mater. Int.*, 2017, **27**, 34–40.
5 M. Hirscher, V. A. Yartys, M. Baricco, J. M. B. Von Colbe, D. Blanchard, R. C. Bowman, D. P. Broom, C. E. Buckley, F. Chang and P. Chen, *J. Alloys Compd.*, 2020, **827**, 153548.
6 E. S. Hanley, J. P. Deane and B. P. Ó. Gallachóir, *Renewable Sustainable Energy Rev.*, 2018, **82**, 3027–3045.
7 N. Z. A. K. Khafidz, Z. Yaakob, K. L. Lim and S. N. Timmiati, *Int. J. Hydrogen Energy*, 2016, **41**, 13131–13151.
8 H. Wang, H. Lin, W. Cai, L. Z. Ouyang and M. Zhu, *J. Alloys Compd.*, 2016, **658**, 280–300.
9 P. E. Dodds, I. Staffell, A. Hawkes, F. G. N. Li, P. Grunewald, W. McDowall and P. Ekins, *Int. J. Hydrogen Energy*, 2015, **40**, 2065–2083.
10 J. B. von Colbe, J.-R. Ares, J. Barale, M. Baricco, C. Buckley, G. Capurso, N. Gallandat, D. M. Grant, M. N. Guzik and I. Jacob, *Int. J. Hydrogen Energy*, 2019, **44**, 7780–7808.
11 R. Moradi and K. M. Groth, *Int. J. Hydrogen Energy*, 2019, **44**, 12254–12269.
12 Y. Gao, N. Zhao, J. Li, E. Liu, C. He and C. Shi, *Int. J. Hydrogen Energy*, 2012, **37**(16), 11835–11841.
13 G. J. Kubas, *Chem. Rev.*, 2007, **107**, 4152–4205.
14 C. Chung, J. Ihm and H. Lee, *J. Korean Phys. Soc.*, 2015, **66**, 1649–1655.
15 U.S. Department of Energy, https://www.energy.gov/eere/fuelcells/doe-technical-targets-onboard-hydrogen-storage light – duty -vehicles.
16 L. Ma, J. Zhang and K. Xu, *Appl. Surf. Sci.*, 2014, **292**, 921–927.
17 H. He, X. Chen, W. Zou and R. Li, *Int. J. Hydrogen Energy*, 2018, **43**, 2823–2830.
18 S. Kumar, M. Samolia and T. J. Dhilip Kumar, *ACS Appl. Energy Mater.*, 2018, **1**, 1328–1336.
19 S. Nachimuthu, P. Lai and J. Jiang, *Carbon*, 2014, **73**, 132–140.
20 L. Yang, L. L. Yu, H. W. Wei, W. Q. Li, X. Zhou and W. Q. Tian, *Int. J. Hydrogen Energy*, 2019, **44**, 2960–2975.
21 P. Tavhare, N. Wadnerkar, V. G. Kalamse and A. Chaudhari, *Acta Phys. Pol., A*, 2016, **129**, 1257–1262.
22 S. Cui, N. Zhao, C. Shi, C. Feng, C. He, J. Li and E. Liu, *J. Phys. Chem. C*, 2014, **118**, 839–844.
23 A. Lueking and R. T. Yang, *J. Catal.*, 2002, **206**, 165–168.
24 A. J. Lachawiec, G. Qi and R. T. Yang, *Langmuir*, 2005, **21**, 11418–11424.
25 D. S. Pyle, E. M. Gray and C. J. Webb, *Int. J. Hydrogen Energy*, 2016, **41**, 19098–19113.
26 M. Blanco-Rey, J. I. Juaristi, M. Alducin, M. J. López and J. A. Alonso, *J. Phys. Chem. C*, 2016, **120**, 17357–17364.
27 C. M. Ramos-Castillo, J. U. Reveles, M. E. Cifuentes-Quintal, R. R. Zope and R. de Coss, *J. Phys. Chem. C*, 2016, **120**, 5001–5009.
28 D. H. Chung, H. Guk, D. Kim, S. S. Han, N. Park, K. Choi and S.-H. Choi, *RSC Adv.*, 2014, **4**, 9223–9228.
29 S. Nachimuthu, P.-J. Lai and J.-C. Jiang, *Carbon*, 2014, **73**, 132–140.
30 A. D. Lueking, G. Psofogiannakis and G. E. Froudakis, *J. Phys. Chem. C*, 2013, **117**, 6312–6319.
31 C.-Y. Wang, J. L. Gray, Q. Gong, Y. Zhao, J. Li, E. Klontzas, G. Psofogiannakis, G. Froudakis and A. D. Lueking, *J. Phys. Chem. C*, 2014, **118**, 26750–26763.
32 T.-Y. Chung, C.-S. Tsao, H.-P. Tseng, C.-H. Chen and M.-S. Yu, *J. Colloid Interface Sci.*, 2015, **441**, 98–105.
33 J. L. Blackburn, C. Engtrakul, J. B. Bult, K. Hurst, Y. Zhao, Q. Xu, P. A. Parilla, L. J. Simpson, J.-D. R. Rocha, M. R. Hudson, C. M. Brown and T. Gennett, *J. Phys. Chem. C*, 2012, **116**, 26744–26755.
34 H. Chen and R. T. Yang, *Langmuir*, 2010, **26**, 15394–15398.
35 T. K. A. Hoang, A. Hamaed, G. Moula, R. Aroca, M. L. Trudeau and D. M. Antonelli, *J. Am. Chem. Soc.*, 2011, **133**, 4955–4964.
36 P. García-Holley, B. Schweitzer, T. Islamoglu, Y. Liu, L. Lin, S. Rodriguez, M. H. Weston, J. T. Hupp, D. A. Gómez-Gualdrón, T. Yildirim and O. K. Farha, *ACS Energy Lett.*, 2018, **3**, 748–754.
37 G. Li, H. Kobayashi, J. M. Taylor, R. Ikeda, Y. Kubota, K. Kato, M. Takata, T. Yamamoto, S. Toh, S. Matsumura and H. Kitagawa, *Nat. Mater.*, 2014, **13**, 802–806.
38 P. Pachfule, A. Acharjya, J. Roeser, T. Langenhahn, M. Schwarze, R. Schomäcker, A. Thomas and J. Schmidt, *J. Am. Chem. Soc.*, 2018, **140**, 1423–1427.
39 T. Mashoff, M. Takamura, S. Tanabe, H. Hibino, F. Beltram and S. Heun, *Appl. Phys. Lett.*, 2013, **103**, 013903.
40 H. Ren, C. Cui, X. Li and Y. Liu, *Int. J. Hydrogen Energy*, 2017, **42**, 312–321.

41 A. A. Ensafi, M. Jafariasl, A. Nabiyan, B. Rezaei and M. Dinari, *Energy*, 2016, **99**, 103–114.
42 Y. Zhou, W. Chu, F. Jing, J. Zheng, W. Sun and Y. Xue, *Appl. Surf. Sci.*, 2017, **410**, 166–176.
43 K. Wenelska, B. Michalkiewicz, X. Chen and E. Mijowska, *Energy*, 2014, **75**, 549–554.
44 S. Ghosh and V. Padmanabhan, *Int. J. Energy Res.*, 2017, **41**, 1108–1117.
45 M. S. Yahya and M. Ismail, *J. Phys. Chem. C*, 2018, **122**, 11222–11233.
46 D. Silambarasan, V. J. Surya, V. Vasu and K. Iyakutti, *ACS Appl. Mater. Interfaces*, 2013, **5**, 11419–11426.
47 P. F. Weck, T. J. Dhilip Kumar, E. Kim and N. Balakrishnan, *J. Chem. Phys.*, 2007, **126**, 094703.
48 A. Deshmukh, R. Konda, V. Kalamse and A. Chaudhari, *RSC Adv.*, 2016, **6**, 47033–47042.
49 P. Li, S. H. Deng, G. H. Liu, L. Zhang, J. Huang and J. Y. Yu, *J. Power Sources*, 2012, **211**, 27–32.
50 R. Y. Sathe, S. Kumar and T. J. Dhilip Kumar, *Int. J. Hydrogen Energy*, 2019, **44**, 6663–6673.
51 M. P. Andrews, S. M. Mattar and G. A. Ozin, *J. Phys. Chem.*, 1986, **90**, 744–753.
52 P. Tavhare and A. Chaudhari, *Indian J. Pure Appl. Phys.*, 2018, **56**, 341–345.
53 K. Judai, M. Hirano, H. Kawamata, S. Yabushita, A. Nakajima and K. Kaya, *Chem. Phys. Lett.*, 1997, **270**, 23–30.
54 D. van Heijnsbergen, G. von Helden, G. Meijer, P. Maitre and M. A. Duncan, *J. Am. Chem. Soc.*, 2002, **124**, 1562–1563.
55 A. D. Becke, *J. Chem. Phys.*, 1997, **107**, 8554–8560.
56 M. J. Frisch, G. W. Trucks, H. B. Schlegel, G. E. Scuseria, M. A. Robb, J. R. Cheeseman, G. Scalmani, V. Barone, B. Mennucci, G. A. Petersson, H. Nakatsuji, M. Caricato, X. Li, H. P. Hratchian, A. F. Izmaylov, J. Bloino, G. Zheng, J. L. Sonnenberg, M. Hada, M. Ehara, K. Toyota, R. Fukuda, J. Hasegawa, M. Ishida, T. Nakajima, Y. Honda, O. Kitao, H. Nakai, T. Vreven, J. A. Montgomery Jr, J. E. Peralta, F. Ogliaro, M. Bearpark, J. J. Heyd, E. Brothers, K. N. Kudin, V. N. Staroverov, R. Kobayashi, J. Normand, K. Raghavachari, A. Rendell, J. C. Burant, S. S. Iyengar, J. Tomasi, M. Cossi, N. Rega, J. M. Millam, M. Klene, J. E. Knox, J. B. Cross, V. Bakken, C. Adamo, J. Jaramillo, R. Gomperts, R. E. Stratmann, O. Yazyev, A. J. Austin, R. Cammi, C. Pomelli, J. W. Ochterski, R. L. Martin, K. Morokuma, V. G. Zakrzewski, G. A. Voth, P. Salvador, J. J. Dannenberg, S. Dapprich, A. D. Daniels, O. Farkas, J. B. Foresman, J. V. Ortiz, J. Cioslowski and D. J. Fox, *Gaussian 09, Revision A.1*, Gaussian, Inc., Wallingford, 2009.
57 R. Car and M. Parrinello, *Phys. Rev. Lett.*, 1985, **55**, 2471–2474.
58 G. Martyna, C. Cheng and M. L. Klein, *J. Chem. Phys.*, 1991, **95**, 1318–1336.
59 B. G. Lippert and J. H. Parrinello, *Mol. Phys.*, 1997, **92**, 477–488.
60 G. Lippert and H. M. Parrinello, *Theor. Chem. Acc.*, 1999, **103**, 124–140.
61 H. B. Schlegel, S. S. Iyengar, X. Li, J. M. Millam, G. A. Voth, G. E. Scuseria and M. J. Frisch, *J. Chem. Phys.*, 2002, **117**, 8694–8704.
62 J. Chai and M. Headgordon, *Phys. Chem. Chem. Phys.*, 2008, **10**, 6615–6620.
63 E_a is the average adsorption energy, k_B is the Boltzmann constant1.38 $\times$ 10^{-23} J K^{-1}, R is the gas constant 8.31 J K^{-1} mol^{-1}, and P is the equilibrium pressure 1 atm, ΔS is the change of the H_2 entropy from gas to liquid phase.